

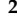




Article

Modeling and Characterization of a Thermally Controlled Iodine Feeding System for Electric Propulsion Applications

Manuel Martín Saravia ^{1,*}, Luca Bernazzani ², Alessio Ceccarini ², Alfio Emanuele Vinci ¹
and Fabrizio Paganucci ¹

¹ Dipartimento di Ingegneria Civile e Industriale, Università di Pisa, Largo Lucio Lazzarino, 56122 Pisa, Italy; a.vinci4@studenti.unipi.it (A.E.V.); f.paganucci@ing.unipi.it (F.P.)

² Dipartimento di Chimica e Chimica Industriale, Università di Pisa, Via Giuseppe Moruzzi 13, 56124 Pisa, Italy; luca.bernazzani@unipi.it (L.B.); alessio.ceccarini@unipi.it (A.C.)

* Correspondence: manuel.saravia@ing.unipi.it

Received: 21 October 2019; Accepted: 15 January 2020; Published: 23 January 2020



Abstract: Iodine is considered as a feasible alternative to xenon as a propellant for electric propulsion systems, thanks to its good propulsive performance, high availability, and high storage density. However, as iodine is stored in solid state at ambient temperature, current state-of-the-art propellant management systems are not suitable to be used with it. Moreover, due to its high reactivity, iodine imposes requirements on material-compatibility, hindering the use of mass flow measurement and control systems typically used with other propellants. The architecture of a controlled iodine feeding system for low power (200 W class) ion and Hall effect thrusters is presented and the resulting prototype is described. It consists of a sublimation assembly whose temperature is used to control the tank pressure, a normally-closed ON-OFF valve, and a thermal throttle to perform the fine control of the mass flow rate. A 1D thermal-fluid model concerning the vapor generation in the tank, and its evolution along the different components is detailed. The thermal throttle model has been experimentally verified using air as a working fluid. The model results agree with the measurements of the verification tests in the hypothesis of the presence of an extended region at the entrance of the pipe where the laminar flow velocity and temperature profiles are not fully developed (known as entry flow region). Finally, the system is experimentally characterized and the model of the full system is calibrated using experimental measurements. The calibration shows that the thermal throttle flow presents an entry flow region, that the viscosity is correctly modeled, and that there is a difference between the measured tank temperature and the effective sublimation temperature.

Keywords: electric propulsion; iodine; propellant management; thermal throttle

1. Introduction

Currently, all operational satellite platforms equipped with Hall and ion thrusters run on xenon or krypton as propellant. Xenon has several useful properties for Electric Propulsion (EP) applications [1], such as high atomic mass, low first ionization energy, and a large ionization cross section, which implies a more efficient generation of the plasma with respect to other options. However, given its increasing application in several high technology industries, its availability and price tend to substantially fluctuate, burdening the development of a space project [2]. Krypton features a better availability and a lower cost, together with an ease of adaptation to heritage systems previously developed for xenon use. However, krypton adoption yields a loss in thrust efficiency and lower storage density with respect to xenon [3]. Noble gases present an additional drawback, as their storage conditions at

supercritical state require a high-pressure tank (of about 150–200 bar), a pressure regulation system and a distribution system to supply the gas at low pressure into the thruster discharge chamber [4]. Being stored in a supercritical state requires complex load operations and introduces safety issues for people involved, limiting also the applicability of this thruster technology in smaller spacecraft, where restrictions on pressurized systems can be a major showstopper. As a consequence, alternative propellants have been investigated, such as condensible metals (i.e., Mg, Zn, Bi, Li) and a non-metallic condensible propellant, iodine [1,4–6]. A successful alternative propellant will allow both reducing the utilization cost and increase the envelope of application of EP technologies. Several properties make iodine a good candidate for replacing xenon in EP applications [1]. As seen in Table 1, its atomic mass of 126.9 amu is close to the 131.3 of xenon and it has similar ionization properties on a monoatomic gaseous state. Iodine allows for solid storage at ambient pressure and below 100 °C at a density of 4.9 g/cm³ (three times the density of supercritical xenon at 200 bar), with an impact on operational and performance issues, such as simpler loading and handling procedures, longer shelf-life, higher specific impulse density, among others [4]. Finally, when comparing cost and availability, iodine presents several advantages with respect to xenon, having a cost of one-fifth that of xenon and a virtually unlimited availability in the high purity required by propulsion systems. However, the chemical reactivity of iodine is one of its main disadvantages. Iodine is a halogen and, in spite of showing the lowest reduction potential within this group, it still can have negative effects on numerous materials of interest for space applications. This feature imposes new constraints on the material selection for propulsion systems and poses significant qualification issues for iodine adoption in space operations. Nevertheless, there is little and sparse information available in the literature referring to how materials used in space behave in the presence of iodine. As a consequence, there are several ongoing efforts aimed at increasing the understanding of the interaction of materials with iodine in a space relevant environment [7,8].

The paper presents the development of the Iodine Feeding System for Electric Thrusters, carried out by the University of Pisa (UniPi) within the framework of the I₂HET Technology Research Program, funded by the European Space Agency (ESA). Section 2 presents the main components of the architecture of a feeding system for electric propulsion, comparing those typically used in noble gas-based systems to those used with condensible propellants, followed by a description of the developed feeding system. Section 3 introduces a physical model aimed at analysing the behaviour of the iodine feeding system and guiding the design activities. Section 4 describes a preliminary test campaign in which air was used as a working fluid to compare the measurements with the predictions of the thermal throttle model. Section 5 outlines the experimental setup used for characterizing the iodine feeding system operation, and explains the methodology for measuring the iodine mass flow rate. Results and discussion are presented in Sections 6 and 7, respectively. Finally, Section 8 summarizes the main conclusions of the activity.

Table 1. Xenon, krypton and iodine properties comparison [1].

Propellant	Xe	Kr	I	I ₂
Atomic (molecular) mass (AMU)	131.3	83.8	126.9	253.8
Ionization Properties				
First, Ionization potential [eV]	12.1	14	10.5	9.3
Peak cross section [10 ⁻¹⁶ cm ²]	4.8	3.7	6.0	12.0
Storage and Handling Properties				
Storage density near room temp. [g/cm ³]	1.6 *	0.5 *	-	4.9
Melting point [°C]	−112	−157	-	113.7
Boiling point at 10 Pa [°C]	−181	−208	-	9
Cost [€/kg]	2000	150	-	480

* 14 MPa and 50 °C.

2. Iodine Feeding System Architecture

2.1. Electric Propulsion Propellant Feeding Systems

State-of-the-art systems based on noble gases use tanks with supercritical conditions to achieve high storage densities, with a pressure between 150 and 350 bars [9–12]. Figure 1 depicts the basic architecture of a noble gas Propellant Management Assembly. In order to deliver the propellant to the thruster unit (i.e., the thruster and the neutralizer), the pressure and the mass flow rate need to be properly regulated, given the important consequences they have on the discharge stability and propulsive performance of the system. After leaving the tank, the gas pressure is reduced to about 2 bar (200 kPa). Then, mass flow controllers further reduce the pressure to about 10 kPa and control the amount of propellant delivered to the thruster and to the neutralizer. Moreover, the system has to provide the components necessary for safe test and loading operations before flight, and proper isolation of the pressurized stages during launch and in case of malfunctions.

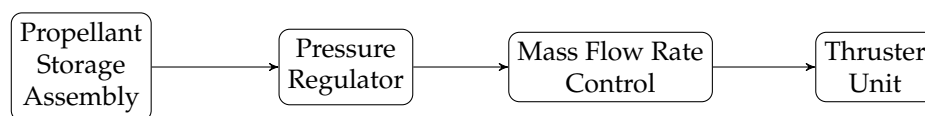


Figure 1. Propellant feeding system basic architecture.

Unlike xenon, iodine is a condensible propellant, which means it can be stored in a solid state in equilibrium with its gaseous phase at room temperature. In this condition, the storage pressure becomes of the order of tenths of Pa. As a result, a high pressure stage is no longer required, and the Iodine feeding system architecture will consist solely of a low pressure phase, formed by a vapor generator and a mass flow controller.

The vapor generator sublimates the solid iodine obtaining vapor at pressure and temperature conditions contained on the solid–gas phase equilibrium line seen in the phase diagram of Figure 2. This means that, instead of requiring a pressure regulation system between the tank and the mass flow control, the pressure at which the propellant leaves the tank can be regulated through the thermal control system of the storage assembly. The result is a much simpler architecture, obtained by merging the two first basic elements into a single pressure regulated storage assembly. This strategy has been applied in the systems developed in the past [5,13–16], in which the temperature of the whole tank is controlled to regulate its internal pressure. These systems provide mass flow control through the use of Proportional Flow Control Valves (PFCV) or Thermal Throttles.

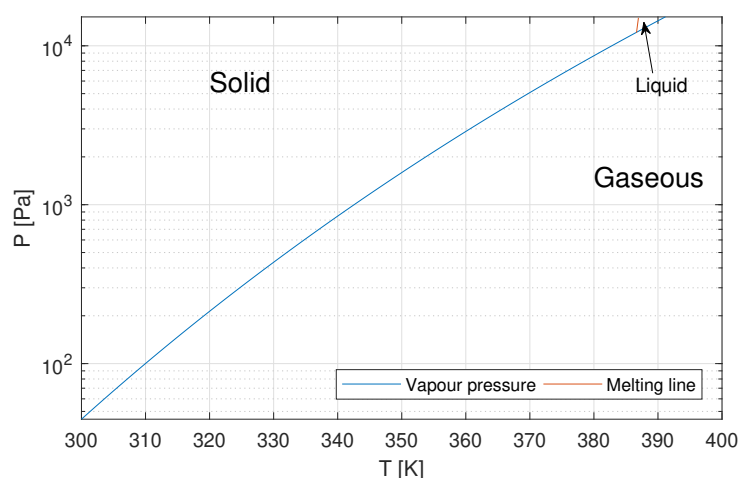


Figure 2. Diatomic iodine phase diagram, according to Antoine Law, as extracted from NIST Chemistry WebBook, SRD 69 [17].

Proportional flow control valves are electromechanical systems that actively change the mass flow rate by opening or closing the flow passage under the command of a feedback control system. PFCVs have fast response times and allow controlling the mass flow rate in a precise way. However, iodine resistant space-rated components are not commercially available and, given their complexity, they would require an expensive development program to obtain a reliable system. Instead, thermal throttles come up as a feasible and relatively inexpensive alternative. Thermal throttling consists of a flow restriction which allows a relatively good fine-tuning of the mass flow rate by changing the viscosity and density of the gas through the control of its temperature. When compared to other methodologies, they stand out for their simplicity and reliability, as no moving parts are involved.

2.2. Developed Iodine Feeding System

As stated before, most iodine feeding systems for electric propulsion developed elsewhere sublime the propellant by heating up the entire tank assembly [5,13–16,18]. On the one hand, this concept has the advantage that iodine is uniformly warmed. However, on the other hand, it implies a large mass is heated, requiring higher powers, complicating the thermal control and increasing the response times. Additionally, microgravity conditions may cause the solid iodine to float freely inside the tank and not have a proper contact with the heating surfaces.

The proposed feeding system architecture, seen in Figure 3a, aims at overcoming these drawbacks, seeking to optimize the use of heating power. It consists of a slender body containing the solid propellant in the form of a cylindrical cartridge. The solid iodine is pushed against the surface of a heated body, called sublimation assembly, which supplies the heat for vaporizing the iodine through one of the bases of the cylinder. The sublimation assembly is a cup-shaped metallic body, whose temperature is measured and controlled by means of electric heaters mounted on the outer surface. Internally, the assembly has a metallic component called filter, which is in close contact with the solid propellant. The filter function is to prevent the propellant grains from entering the sublimation body and to convey the heat directly to the solid-vapor interface. A piston, pushed by a spring, provides the force to keep the iodine in contact with the filter. After evaporation, the iodine flows into the cavity of the sublimation assembly, which acts as a plenum, providing some damping in case of mass flow rate oscillations. The rest of the feeding system consists of an ON-OFF valve and a thermal throttle for the fine mass flow control. The thermal throttle consists of a capillary pipe whose temperature is controlled to finely regulate the mass flow rate. Its dimensions are selected to assure the flow reaches sonic conditions at the exit section, allowing to decouple the flow close to the sublimation surface from any fast downstream oscillation that may occur and that could affect the controllability of the flow.

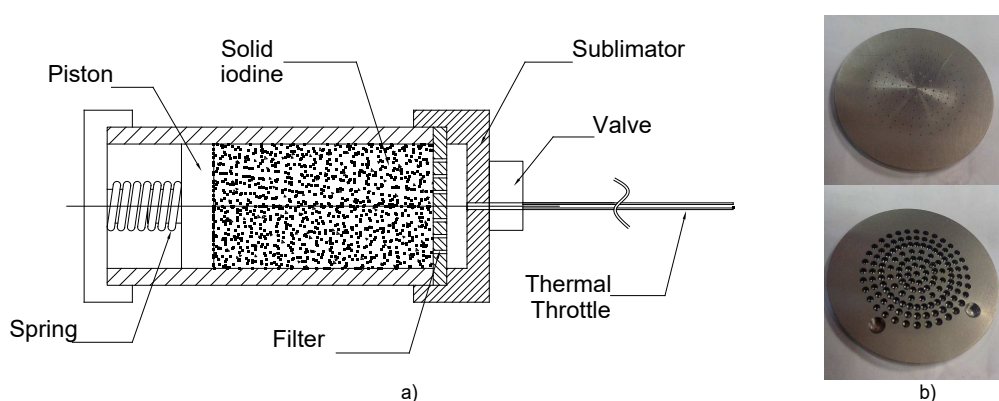


Figure 3. (a) Proposed feeding system architecture; (b) Inconel filter.

As stated before, the gross regulation of the mass flow rate is made by controlling the sublimation pressure through the temperature of the sublimation body, and the fine control by means of the thermal throttle. The main features of this concept are:

- Low power requirements, as only a small surface of the iodine is heated and power loss towards the base of the tank is limited by the low thermal conductivity of iodine;
- absence of significant thermal control issues at a system level, given that only a small part of the system is at high temperature and can be easily insulated;
- short response time, between 20 and 30 min at start up, since the involved thermal inertia are small;
- control requirement only on the temperature of the system, simplifying diagnostics and control;
- reliability, as the valve is the only active component;
- good throttleability; and
- scalability.

The filter is a critical component, as it is exposed to the harsh environment of hot dense iodine vapor. It consists of an Inconel X-750 filter with 137 holes with a diameter of 0.26 mm, shown in Figure 3b.

3. Feeding System Physical Model

To gain insight on the physical processes occurring within the feeding system, and to have a useful tool for guiding the sizing of the system, a thermal-fluid model capable of predicting the iodine mass flow rate as a function of the temperature on the sublimation surface and of the thermal throttle wall has been developed. The model considers the feeding system as divided in three consecutive stages and four corresponding stations, as shown in Figure 4a:

- Station (1)** Sublimation of a finite mass flow rate from a surface at close-to equilibrium condition, defined according to the Clausius–Clapeyron relation between pressure and temperature, corrected by the presence of a finite mass flow rate. The iodine mass flow rate is expressed as a function of heat power input and vapor thermodynamic properties.
- Stage (1–2)** Isothermal flow through a multi-perforated metallic filter.
- Stage (2–3)** Isothermal flow along the plenum between the filter and the coupling PTFE (Teflon®) pipe inlet.
- Stage (3–4)** Compressible viscous flow with heat exchange and fixed wall temperature along the valve coupling pipes (D_3) and the capillary pipe (D). The valve introduces a concentrated pressure loss. Between the points in which the PTFE and the capillary pipe the area changes an isothermal flow with area change is considered, as in Stages 2–3.
- Station (4)** Sonic condition at the capillary pipe exit, decoupling upstream from downstream flow.

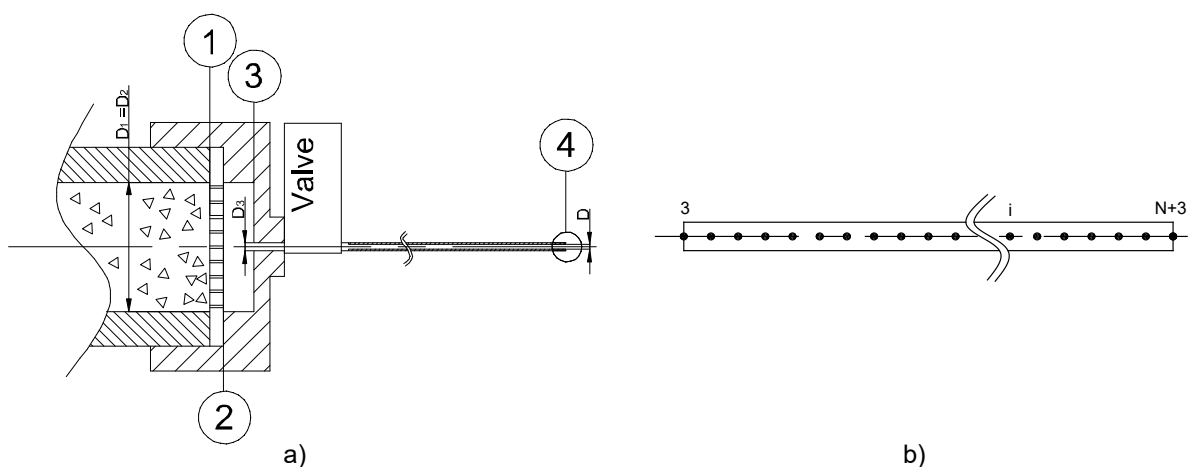


Figure 4. (a) Model geometry; (b) geometry of the thermal throttle model.

The problem is mathematically defined by a set of algebraic and differential equations that relate the values of pressure (P_i), velocity (V_i) and temperature (T_i) in each stage or station.

3.1. Tank Model

The Stages (1–3) that include the iodine vaporization and flow along the tank plenum are the following:

(1) Sublimation at the solid iodine column:

At this station, there is a situation in which solid iodine is close to equilibrium with its gaseous phase, whose pressure is related to the finite mass flow rate by the law used by Polzin et al. in [18]:

$$P_1 = P_{vap} - \frac{\dot{m}}{\alpha A} \sqrt{2\pi RT_1} \quad (1)$$

in which P_{vap} is the vapor pressure in an equilibrium condition, α is the sticking coefficient (usually assumed close to 1), R is the gas constant for molecular iodine (equal to 32.76 J/kg/K), and A is the exposed surface of the iodine cartridge. The vapor pressure, can be defined by the Clausius–Clapeyron relation:

$$P_{vap} = P_{ref} e^{-\frac{\Delta h_s}{R} \left(\frac{1}{T_1} - \frac{1}{T_{ref}} \right)}, \quad (2)$$

where P_{ref} and T_{ref} are arbitrarily chosen reference values along the curve (the reference temperature is 373.15 K, and its corresponding reference pressure is 5993 Pa, as taken from the empirical curve defined by the Antoine relation [17]) and Δh_s is the iodine sublimation heat (assumed constant with a value of 245.86 kJ/kg [17]).

The total power input coming from the hot filter is split into two main contributions: (i) Q_I , the time varying heat power transferred by conduction inside the solid iodine and the wall (not considered in the present problem), and (ii) Q_S , the heat power actually used for sublimation. Q_S is proportional to the iodine mass flow rate, so that the following relationships among Q_S , P_1 , V_1 and T_1 hold:

$$\dot{m} = \frac{\dot{Q}_S}{\Delta h_s} \Rightarrow V_1 = \frac{\dot{m}}{\rho_1 A_1}, \quad (3)$$

where $\rho_1 = P_1 / (RT_1)$.

(2) Isothermal flow through the filter:

The vapor goes through the metallic filter in a process assumed to be isothermal, at the sublimation temperature.

$$\begin{cases} P_2 = P_1 \left(1 - \frac{\zeta (A^*/A) V_1^2}{2RT_1} \right), \\ V_2 = V_1 \left(\frac{P_1}{P_2} \right), \\ T_2 = T_1. \end{cases} \quad (4)$$

ζ is a coefficient relating the static pressure loss with the dynamic pressure of the flow. It is a function of the total passage area along the holes and the area of the filter [19]. In this case $(A^*/A) = 0.043$, which yields a $\zeta \simeq 1500$.

(3) Isothermal flow along the plenum:

Considering the mass and momentum equation of a compressible flow, and a constant temperature, one obtains the system of equations that allow solving for the section change between the plenum and the thermal throttle entrance:

$$\begin{cases} P_3 = P_2 \frac{1 + \frac{V_2^2}{RT_2} \left(\frac{D_2}{D_3}\right)^2}{1 + \frac{V_3^2}{RT_3}}, \\ V_3 = V_2 \frac{P_2}{P_3} \frac{T_3}{T_2} \left(\frac{D_2}{D_3}\right)^2, \\ T_3 = T_2. \end{cases} \quad (5)$$

3.2. Thermal Throttle Model

The flow of gas along thermal throttles consisting of capillary pipes has been considered as a Poiseuille flow in [5]. This model allows for quick sizing of a thermal throttle, but the assumption of constant density hinders its applicability to cases in which the sonic condition is achieved in the exit. As a consequence, a more elaborate model that considers changes in density becomes necessary. The implementation of the model starts from the steady Navier–Stokes equations for a compressible 1D flow. Then, through the use of the Shapiro–Hawthorne influence coefficients method, detailed in [20], a simple set of expressions is obtained, in which effects of friction and heat exchange with the wall are considered. The model assumes that the flow is laminar, the wall temperature is uniform all along the pipe, the gas is calorically perfect (C_p is constant) and that the changes in the stream properties are continuous, i.e., no shocks are present, which is always true as the flow remains subsonic all along the domain. Additionally, the fact of having $M < 1$ allows us to consider, without incurring in large errors that there is no considerable difference between the adiabatic wall temperature and the stagnation temperature, i.e., that the recovery factor is unity [20]. To consider the gas calorically perfect is accepted as large local variations of temperature are not expected.

The hypothesis of laminar flow implies that (Ref. [21]):

- the Nusselt number, i.e., the ratio between convective and conductive heat transfer, is $Nu = 3.66$ (entry flow effects are neglected); and
- the friction factor will be a function of the Reynolds number, as $f = \frac{16}{Re}$.

The result is a set of three differential equations relating the velocity, the static temperature and the stagnation pressure with initial conditions in the pipe entry. The set, expressed in logarithmic differential form, is:

$$\begin{cases} \frac{dP_0}{P_0} = -\frac{\gamma M^2}{2} \left[\frac{dT_0}{T_0} + F_{fr} \right], \\ \frac{dV}{V} = \frac{1}{1-M^2} \left[\frac{dT_0}{T} + \frac{\gamma M^2}{2} F_{fr} \right], \\ \frac{dT}{T} = \frac{1}{1-M^2} \left[(1 - \gamma M^2) \frac{dT_0}{T} - \frac{\gamma(\gamma-1)M^4}{2} F_{fr} \right], \end{cases} \quad (6)$$

with:

$$P = \rho RT \quad M = \frac{V}{\sqrt{\gamma RT}} \quad (7)$$

and

$$P_0 = P \left(1 + \frac{\gamma-1}{2} M^2 \right)^{\frac{\gamma}{\gamma-1}} \quad T_0 = T \left(1 + \frac{\gamma-1}{2} M^2 \right). \quad (8)$$

The factor F_{fr} includes both the friction effect with the walls and concentrated losses, such as the one occurring along the valve, characterized by ζ_v that represents the ratio of the pressure loss over the dynamic pressure:

$$F_{fr} = \frac{4f dx}{D} + \zeta_v. \quad (9)$$

3.3. Numerical Implementation

The precedent equations include properties that are a function of the local temperature, such as the viscosity and the thermal conductivity, so an analytical solution is not possible. To implement a numerical solution, the equations are discretised using a finite difference forward scheme:

$$d\phi = \phi_{i+1} - \phi_i. \quad (10)$$

In this way, the domain of the pipe is divided in N segments along which the parameters are considered constant, as in Figure 4b.

To calculate the change of total temperature along one segment, we express the change in total temperature as:

$$\dot{m}C_p dT_0 = \dot{q}_w dA_w. \quad (11)$$

Assuming that the flow is laminar, we can express the heat flux through the wall as (from [21]):

$$\dot{q}_w = \frac{Nu_w \lambda (T_w - T_0)}{D}, \quad (12)$$

where Nu_w is the Nusselt number for the heat transfer through the wall, λ is the thermal conductivity of the fluid, and T_w is the wall temperature in the thermal throttle. Introducing the definition of the heat flow through the walls in Equation (11) and, as we consider the wall temperature T_w to be constant, we can express the change of T_0 as the change in the difference with respect to the wall:

$$dT_0 = d(T_0 - T_w) = \frac{Nu_w \lambda (T_w - T_0) \pi D dx}{\dot{m}C_p D}. \quad (13)$$

Rearranging the terms and integrating between the extremes of a segment:

$$\ln \frac{(T_0 - T_w)_{i+1}}{(T_0 - T_w)_i} = - \frac{Nu_w \lambda \pi (x_{i+1} - x_i)}{\dot{m}C_p}. \quad (14)$$

Finally, the change of total temperature along one segment results in:

$$(\Delta T_0)_i = (T_w - T_{0i}) \left[1 - \exp \left(- \frac{Nu_w \lambda (T_w - T_{0i}) \pi (x_{i+1} - x_i)}{\dot{m}C_p} \right) \right]. \quad (15)$$

The friction effects represented in Equation (9) are considered by introducing the Fanning friction factor for a laminar flow in a circular pipe ($f = 16/Re_D$), and expressing the Reynolds number as a function of the local flow parameters, the term F_{fr_i} can be expressed as:

$$F_{fr_i} = 64 \frac{\mu(T_i)}{\rho_i V_i} \frac{(x_{i+1} - x_i)}{D^2} + \zeta v_i. \quad (16)$$

In expressions (15) and (16), the dynamic viscosity and the thermal conductivity are a function of the temperature, which is evaluated at the beginning of the segment.

Finally, the resulting set of equations is:

$$\begin{cases} P_{0i+1} &= P_{0i} - \frac{\gamma M_i^2}{2} P_{0i} \left[\frac{(\Delta T_0)_i}{T_{0i}} + F_{fr_i} \right], \\ V_{i+1} &= V_i + \frac{V_i}{1-M_i^2} \left[\frac{(\Delta T_0)_i}{T_i} + \frac{\gamma M_i^2}{2} F_{fr_i} \right], \\ T_{i+1} &= T_i + \frac{T_i}{1-M_i^2} \left[(1 - \gamma M_i^2) \frac{(\Delta T_0)_i}{T_i} - \frac{\gamma(\gamma-1)M_i^4}{2} F_{fr_i} \right]. \end{cases} \quad (17)$$

These equations are defined for a set of nodes along the entire pipe (500 nodes are used to discretize the domain). The model solution assumes R equal to 32.759 J/kg/K and C_p is assumed constant and equal to 146.4 J/kg/K. γ is equal to 1.28, as calculated from the values of C_p and R . The variation of viscosity with temperature has been modeled in accordance with Chung et al. [22,23]. This model relies on the Chapman–Enskog gas kinetic treatment which considers the interactions between colliding molecules by way of an intermolecular potential and includes an additional factor to account for molecular shapes and polarities [24]. The underlying assumptions of the theory make the model applicable only to low-pressure, high-temperature gases, as is the case of interest since the feeding system works below the triple point. The relation is:

$$\mu = \frac{40.785 F_c(\omega, \eta_r) (\mathcal{M}T)^{1/2}}{V_c^{2/3} \Omega_v} \cdot 10^{-7} \quad [\text{Pa} \cdot \text{s}], \quad (18)$$

where $F_c(\omega, \eta_r)$ is a correction factor accounting for molecular shape and polarity through the acentric factor ω and the reduced dipole moment η_r , as detailed in [24], while \mathcal{M} is the molar mass in g/mol, T is the temperature in K, V_c is the critical volume in cm³/mol, and Ω_v is the collision integral [25]. The used thermal conductivity model also follows Chung et al. [22,23] on the basis of what is proposed by Mason et al. in [26] for polyatomic low-pressure gasses. The relation is:

$$\lambda = 3.75 \Psi R \mu \quad [\text{W} / (\text{m} \cdot \text{K})], \quad (19)$$

where Ψ is a function of c_v , reduced temperature T_r and acentric factor ω , as explained in [24], R is the specific gas constant in J/(kg·K), and μ is the low-pressure gas viscosity in Pa·s.

The model is solved by means of a shooting method for a certain pair of set-point values for the sublimation body temperature T_1 and a thermal throttle temperature T_w . Having set these temperatures, a value of Q_5 is proposed. The equations are solved advancing towards the exit until the last node. The values of P_4 , V_4 , and T_4 are thus obtained. With these values, the value of M_{exit} is calculated. In case $M_{exit} = 1$ is not verified at the throat, Q_5 is corrected and the calculations are restarted with this new value, repeating until convergence to the sonic condition is attained. The output of the solution is a distribution of P , V and T along the whole system. An example of the results is shown in Figure 5.

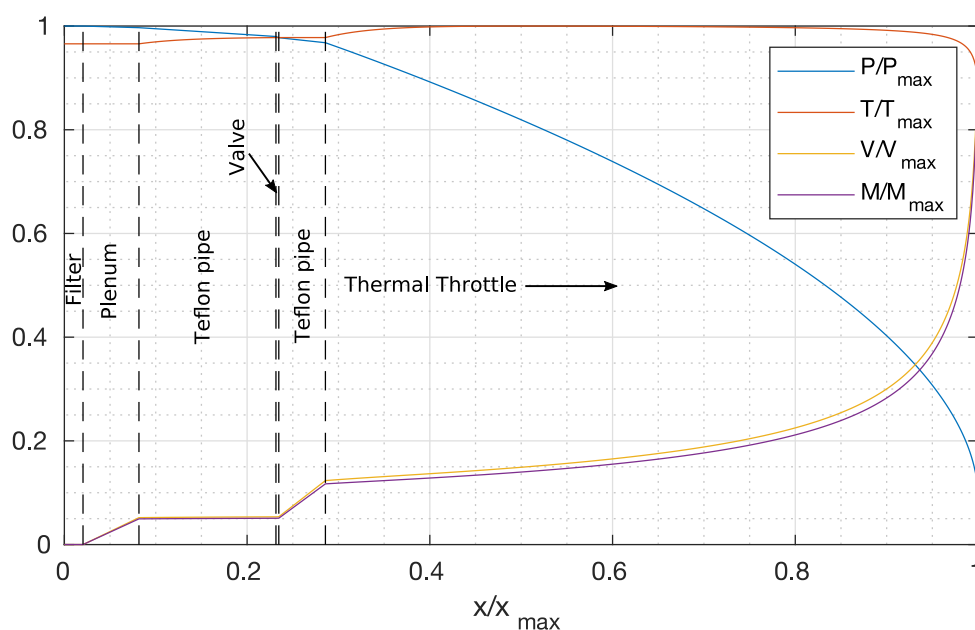


Figure 5. Normalized properties distribution along the feeding system.

4. Thermal Throttle Preliminary Tests with Air

A series of tests were performed aimed at contrasting the thermal throttle model with experimental measurements. The experiment consists in measuring the air mass flow rate passing through a heated capillary pipe at different pipe temperatures. A fused silica gas chromatography tube with an internal diameter of 0.53 mm and a length of 200 mm was mounted inside an Inconel pipe. The external pipe had a coupling for the silica tube on one extreme and was open on the other. The Inconel tube is wrapped with a constantan wire for heating, while a Pt100 thermistor measures its temperature with an accuracy of 1 °C. The pipe was mounted on a stainless steel support, whose temperature was also controlled, so as to have a uniform temperature along the pipe length. The device has been placed in a vacuum chamber, as shown in Figure 6a. The pipe inlet has been connected to the atmosphere by means of a fluidic feedthrough. A mass flow meter (mod. EL-FLOW, by Bronkhorst, Ruurlo, The Netherlands) has been placed between the feedthrough and the atmosphere. A vacuum in the chamber, of the order of 1 Pa, assures choking condition at the pipe exit. The mass flow meter measures the air flow with an accuracy better than 0.05 mg/s. As the air comes from the atmosphere, the total pressure and temperature of the working fluid could be easily known at the pipe inlet from measurements of the laboratory atmospheric conditions.

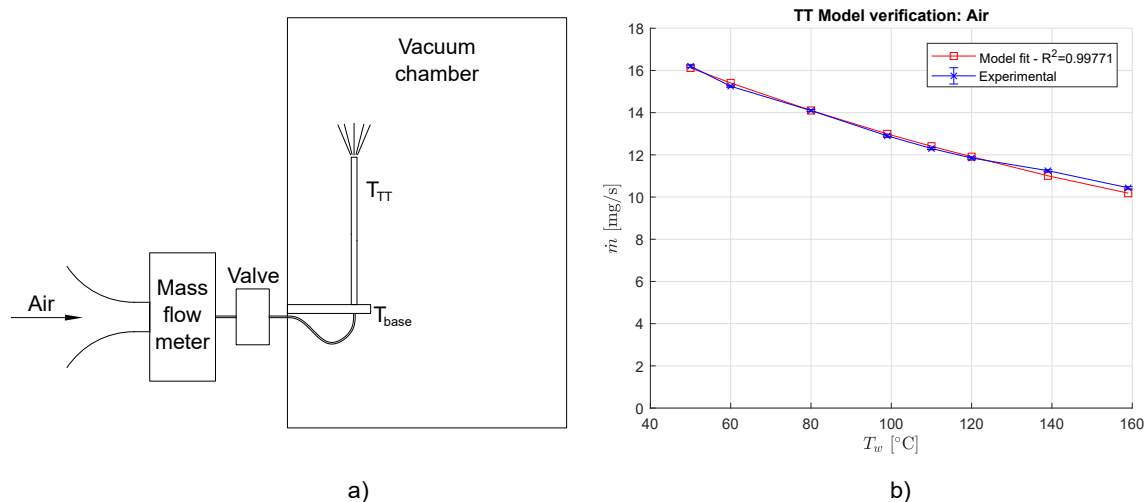


Figure 6. Test with air: (a) setup scheme; (b) results and model fit.

4.1. Results

During the test, the temperature of the block and the pipe were varied together from 40 to 160 °C with a step of 20 °C. At the lowest temperature set point, the thermal throttle could not be properly controlled as the thermal inertia was too low for the available power input, resulting in a difference of 10 °C between the setpoint and the measured value. The external air temperature was also registered, as it corresponds to the total temperature of the working gas. Table 2 and Figure 6b present the measured mass flow rates as a function of the pipe temperature. From the test results, it is evident that the thermal throttle is capable of accurately modulating the mass flow rate by means of the variation of the pipe temperature.

Table 2. Results of thermal throttle test with air.

		Set Point			Measurement		
P_{in} [hPa]	T_{in} [°C]	T_{Base} [°C]	T_{tt} [°C]	T_{Base} [°C]	T_{tt} [°C]	\dot{m} [mg/sec]	P_{VC} [mbar]
1008 ± 5	24	40	40	40	50	16.2	7.6
	24	60	60	60	60	15.25	7.5
	24.5	80	80	80	80	14.1	7.45
	24	100	100	99	99	12.9	7.4
	24.5	120	120	120	110	12.3	7.3
	24	120	120	120	120	11.85	7.3
	24.5	140	140	139	139	11.25	7.25
	24	160	160	160	159	10.44	7.2

4.2. Discussion

To gain insight in the processes involved in the evolution of the flow, the model and the experimental results were fitted using a Bayesian approach to data analysis (see [27,28] for a description of the Bayesian approach to Data Analysis; the parameter fitting routine implemented is based on the nested sampling method [29,30]). Free calibration factors were added to the model to account for the uncertainty of gas viscosity and of Nusselt number:

$$\mu_{fit} = K_1 \cdot \mu(T_i) \quad Nu_{fit} = K_2 \cdot Nu_w. \quad (20)$$

The data analysis yielded a calibration factor K_1 equal to 0.99 ± 0.015 for the viscosity, showing that the model used to calculate this parameter was appropriate. Regarding the heat transfer, the analysis showed that $K_2 = 1.65 \pm 0.6$, resulting in an effective Nusselt number equal to 6, possibly due to an entry region flow in the capillary tube where the laminar flow was not completely developed neither kinematically nor thermally. This results in a higher average Nusselt number, as shown in Figure 7 (see Chapter 8.4 of [31] for further details). Model calculations made using the corrected value of Nusselt number showed that the Prandtl number at the inlet of the capillary pipe is 0.7 and the entry length is between 5 and 6 mm, so the flow is not fully developed for at least 10 pipe internal diameters. It is worth remarking that the model considers a constant Nusselt number for the whole length of the pipe. This is not completely accurate, as for positions beyond the entry region its value should be 3.66. However, most of the heat exchange occurs when the gas enters the pipe and the temperature difference between the gas and the wall is the highest, so the global Nusselt number value will be mostly dominated by the value of the entry region.

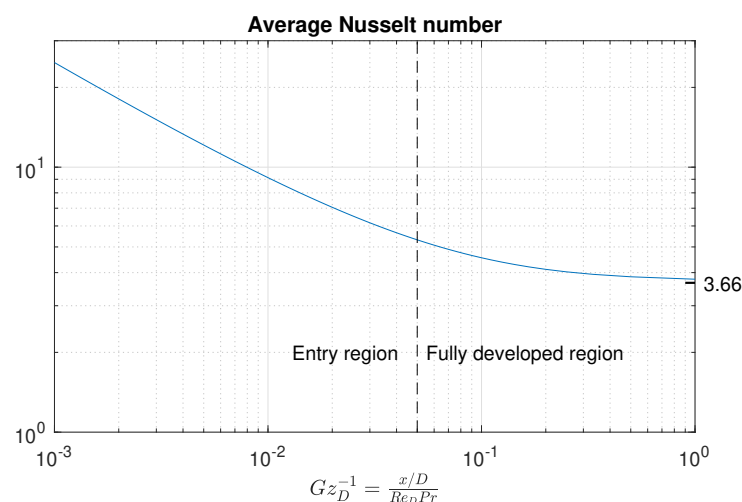


Figure 7. Average Nusselt number for entry region ($Pr = 0.7$), according to Baehr and Stephan correlation, as extracted from [31].

The comparison of experimental values with those obtained using the calibrated model show that the thermal throttle model manages to adequately catch the phenomena occurring during the evolution of the flow.

5. Feeding System Test

5.1. Feeding System Prototype

The Iodine Feeding System described in Section 2 and modelled in Section 3 was built and the prototype is shown in Figure 8a. Seeking to reduce the stress induced on the valve thread by thermal deformation of the system, additional PTFE pipes with an internal diameter of 0.8 mm and 10 mm long was added between the sublimation body and the valve and 5 mm between the valve and the capillary pipe coupling. The presence of this pipe segment was included in the physical model considering the same approach as the capillary pipe, and assuming an isothermal flow when the diameter of the pipe changes.

The thermal throttle consists of a fused silica capillary pipe 70 mm long and 0.53 mm of internal diameter. Pt100 thermistors were mounted on the sublimation and the thermal throttle assemblies to measure their temperatures and use them as input in a set of Gefran 1350 PID controllers (by Gefran SpA, Provaglio d'Iseo, Italy) that regulated the system temperatures. The temperature of the valve was controlled by means of a T-type thermocouple and a heating resistor, making sure that it remained always higher than the sublimation assembly temperature, so as to avoid the condensation and clogging of the valve. Additionally, type-T thermocouples were mounted on the sublimation assembly and on the thermal throttle to verify and backup the measurements made with the thermistors. These temperature measurements were registered using a Keysight 34970A/34972A Data Acquisition unit (by Keysight Technologies Inc., Colorado Springs, CO, USA), with a multiplexer card and yielded a resolution of 0.1 °C and are those taken as a reference for the test results.

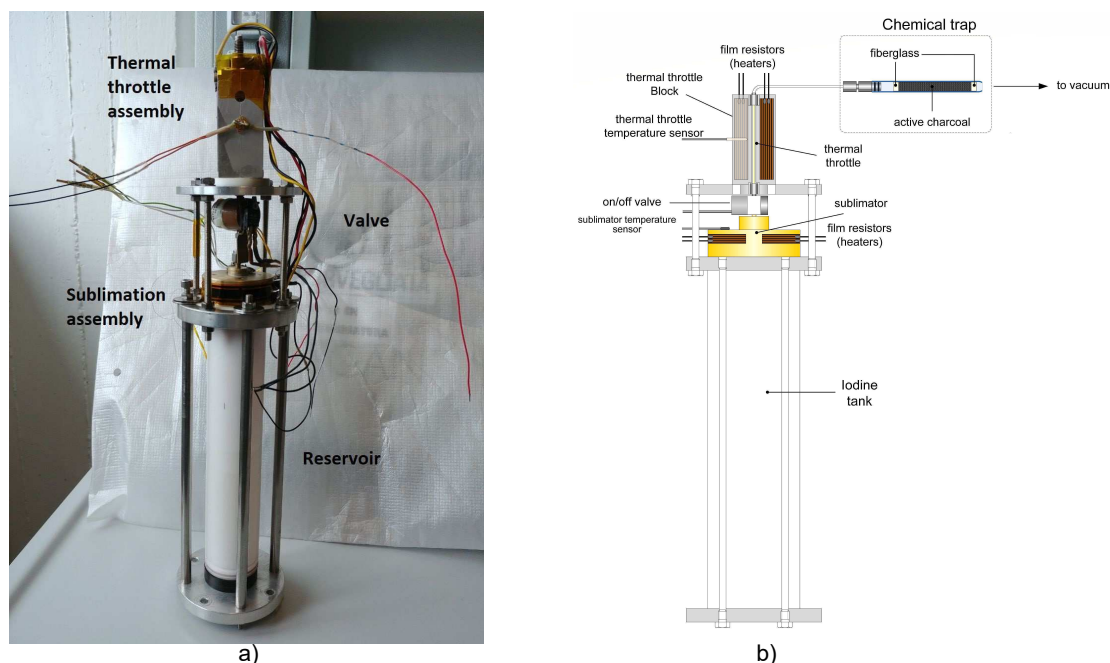


Figure 8. (a) Iodine Feeding System prototype; (b) test setup.

5.2. Vacuum Facility and Iodine Collection Method

The whole system was mounted and operated in a stainless-steel modular vacuum chamber in the Physical Chemistry laboratory, at the Department of Chemistry and Industrial Chemistry (DCCI) of the Università di Pisa. The chamber is equipped with a Vacsound D12 rotary vane pump (by

Galileo Vacuum Tec, Scandicci, Italy). The pressure is measured using a Galileo Vacuum Tec OG120 gauge. The minimum pressure achieved by the system is 3×10^{-2} mbar (3 Pa) with the test item mounted inside.

In case of dispersion of iodine inside the chamber, a LN2 cold trap is used to keep it from arriving into the pump, where it can dissolve in the oil and eventually damage the components. This method has proved to be an effective manner to both protect the vacuum pump and to easily detect iodine leaks or malfunctions of the feeding system, thanks to the capacity to quickly put in evidence when iodine condensates on the trap wall.

Chemical traps are used to measure average iodine mass flow rates at different test conditions. A chemical trap consists of a glass phial loaded with active charcoal, connected on one end to the thermal throttle and opened to the vacuum chamber on the other, as shown in Figure 8b. When the temperatures of the different parts of the system reach a steady condition, the valve is opened for a given time, between 1 and 10 min, during which the iodine is absorbed by the charcoal. The mass of iodine gathered by the trap is obtained by measuring the mass of the trap before and after the test. The change in weight of the trap is then measured using a technical balance with a resolution of 10^{-4} g. The average mass flow rate is then calculated as the ratio between the trap weight change and the time the valve remained open. In case a trap saturates and iodine goes through without being absorbed, it deposits on the cold trap and the measurement is discarded. This method for measuring the mass flow rate has demonstrated good repeatability and an accuracy of 0.05 mg/s or less, regardless the opening time or the mass of charcoal loaded [32].

For this test campaign, the tank was loaded with 50 g of bi-sublimated iodine grains with a purity larger than 99.8%.

5.3. Test Procedure

The procedure consisted of setting the operative point, i.e., a sublimation body and a thermal throttle temperature (see Table 3), and wait until the temperatures of the different components are settled. The phial is loaded with active charcoal and then is connected to the iodine line and the vacuum chamber is closed. Then, the valve connecting the vacuum line to the chamber is opened and the pressure descends to 3 Pa. Upon pressure stabilization, the system valve is opened to start the iodine flow. After the desired time, the feeding system valve is closed. Afterwards, the chamber is vented and the phial is extracted, sealed to avoid affecting the measurement with the evaporation of iodine or the adsorption of humidity, and weighted. Each point is repeated at least three times.

Table 3. Tested temperature set-points.

T Sublimation Body [°C]	T Thermal Throttle [°C]
104	108
	110
	112
100	110
	105
	102
98	110
	105
	100
94	110
	105
	100
90	110
	105
	100

6. Results

Table 4 and Figure 9 present the test results. It can be seen that the system manages to generate and control the iodine mass flow rate, within a margin of 0.057 mg/s for a wide range of operative regimes.

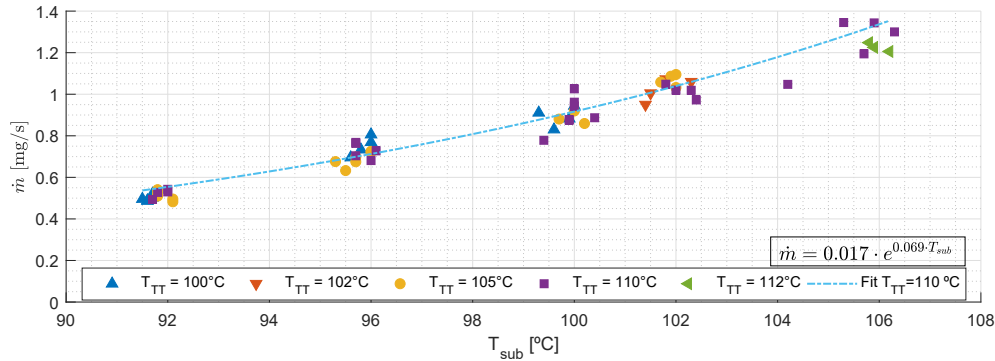


Figure 9. Mass flow rate measurements vs. sublimation body temperature.

Table 4. Aggregated test results.

T Sublimation Body	T Thermal Throttle [°C]	Average \dot{m}	Std. Dev. \dot{m}	
[°C]	[°C]	[mg/s]	[mg/s]	%
91.6	100.3	0.499	0.014	2.76
91.9	105.3	0.511	0.023	4.49
91.9	110.3	0.523	0.021	4.00
95.9	101.1	0.751	0.047	6.30
95.7	105.3	0.688	0.034	5.00
95.8	110.3	0.729	0.038	5.17
99.9	108.8	0.908	0.073	8.03
100.0	105.0	0.886	0.031	3.50
99.8	100.0	0.886	0.057	6.45
102.1	110.0	1.015	0.031	3.09
101.9	105.0	1.068	0.029	2.67
101.8	102.0	1.022	0.056	5.49
106.0	112.0	1.227	0.021	1.73
105.8	110.0	1.296	0.071	5.46
105.7	108.0	1.283	0.023	1.80

7. Discussion

The tests showed the system architecture is capable of generating and controlling a flow of iodine within an accuracy of 0.057 mg/s. Similarly to the case of the thermal throttle test performed with air, the experimental results were fitted using the physical model within a Bayesian framework so as to gain further insight on the processes evolving inside the system. Considering that the measured mass flow rates were lower than those originally expected, and together with thermal analysis of the sublimation assembly, it is likely that the vaporization of iodine occurs at temperature lower than those measured externally with the thermocouples, $T_{sub,TC}$. Moreover, the analysis showed that the difference between the temperatures grew for larger setpoint temperatures. To take this effect into account, in addition to the parameters K_1 and K_2 accounting for the uncertainty in the viscosity and the Nusselt number, the difference between the externally measured temperature and the effective sublimation temperature was taken into account as a linear function of the measured temperature, defined by the values ΔT_{max} and ΔT_{min} :

$$T_{sub,eff} = T_{sub,TC} - \left[\Delta T_{min} + \frac{\Delta T_{max} - \Delta T_{min}}{106 - 91.6} (T_{sub,TC} - 91.6) \right]. \quad (21)$$

Using these four parameters, the model was adjusted, as seen in Figure 10, with the resulting calibration parameters shown in Table 5. It can be seen that the K_1 coefficient, relevant to the viscosity, is close to 1. A previous version of the fluid model, described in [33], relied on a Sutherland approximation of the viscosity as a function of temperature, as proposed in [34]. However, this approximation systematically underestimated the viscosity value for temperatures below the triple point by almost 40%, so that K_1 was always significantly larger than 1. Consequently, we argue that the viscosity model herein introduced can be considered an improvement with respect to the Sutherland approximation.

With respect to the thermal effects in the flow, a global Nusselt number of about 13.4 implies the entry region effect is likely present. If we compare this value to that of the experiments performed with air, it is likely that the entry region represents a larger fraction of the tube length. This occurrence could be expected, as the pipe length is almost one third of that of the pipe used in the tests with air.

Regarding the difference between the temperature measured on the sublimation body outer wall and the effective sublimation temperature, it can be seen that it varies between 5.2 and 11 °C. This occurrence is in line with numerical thermal model results [35]. However, a confirmation can be obtained in future experimental activities in which the temperature on the solid iodine surface will be measured.

Table 5. Tested temperature set-points.

T Sublimation Body [°C]	T Thermal Throttle [°C]
K_1	1.012 ± 0.29
K_2	3.67 ± 1.4
ΔT_{min}	5.2 ± 2.7
ΔT_{max}	11.0 ± 2.5

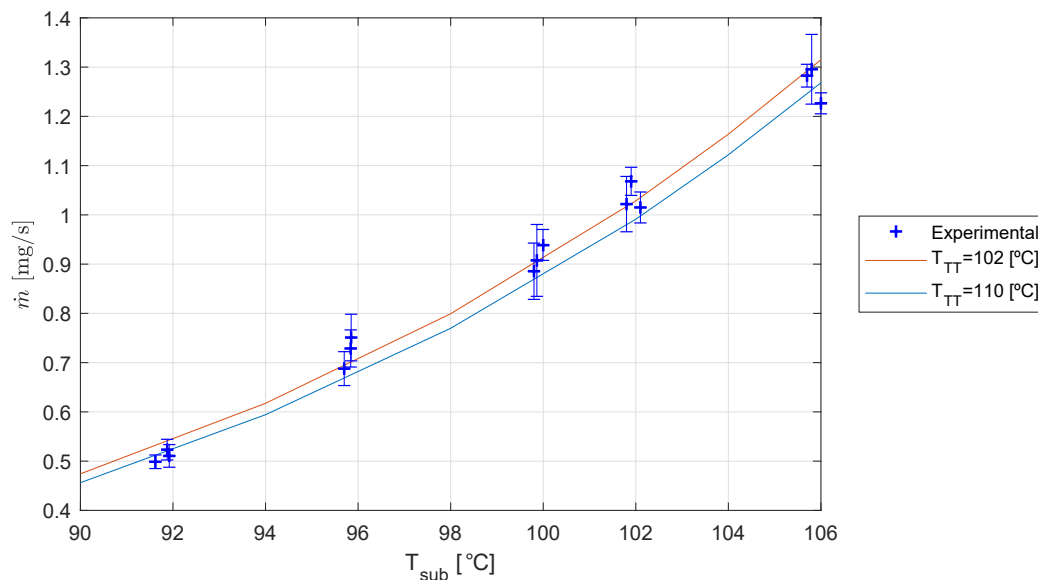


Figure 10. Experimental points and calibrated model curves.

The observation of Figure 10 shows that, after calibration, the model and the experimental results correlate acceptably. It also shows that, as the mass flow rate increases, the thermal throttle control capability also grows, i.e., the mass flow rate variation it can produce is larger. As a consequence, higher operative temperatures should be attempted in the future to increase the thermal throttle capacity.

8. Conclusions

Iodine has proved to be an interesting alternative propellant for low power electric propulsion applications. Its condensible nature brings up the necessity of new systems for the storage, generation and delivery of the propellant to the thruster unit. This article introduces a novel feeding system architecture that stores, sublimates and controls the mass flow rate of iodine with reduced heating power use. A thermal throttle is proposed for fine-tuning the mass flow rate and for decoupling the downstream effects from the tank.

A theoretical model, useful both for analytical purposes and for guiding the design process, is presented and discussed. The approach for modeling the thermal throttle was experimentally verified using air as a working fluid. The experiments showed that the proposed thermal throttle setup was capable of controlling the mass flow rate. Moreover, the correlation between the model and the experiments showed that it is likely that an entry flow region is present, as the average Nusselt number proved to be larger than the 3.66 value expected for a fully developed laminar flow.

The prototype of the feeding system underwent an experimental campaign intended to characterize its behavior regarding the iodine flow generation and control. The system demonstrated its capability of generating a mass flow rate between 0.5 and 1.3 mg/s and of controlling this value with an accuracy of 0.057 mg/s. The correlation of the experimental data with the model showed that the viscosity model used is appropriate, and that the shorter pipe used in the iodine experiment presents a more extended entry flow region when compared to the air experiment. Finally, the theoretical model indicated that there is a difference between the sublimation assembly temperature measured on the external wall and the temperature at which the sublimation actually takes place on the solid–vapor interface. This occurrence is consistent with what was observed in a numerical thermal model. Nevertheless, it is expected to further investigate this effect in future experimental activities.

Author Contributions: Conceptualization, F.P. and L.B.; methodology, A.C. and L.B.; resources, A.C.; investigation, M.M.S. and A.E.V.; data curation, M.M.S. and A.E.V.; writing—original draft preparation, M.M.S.; writing—review and editing, F.P., A.E.V., and L.B.; supervision, A.C.; project administration, F.P.; funding acquisition, F.P. All authors have read and agreed to the published version of the manuscript.

Funding: This research was funded by the European Space Agency in the framework of the contract 4000119530/17/NL/PS “Use of Iodine as Propellant for Hall Effect Thrusters”.

Acknowledgments: We would like to express our gratitude to Marcello Mininni, Avantika Garde, Tatiana Boulzaguet, Alberto Sarritzu, and Laura Capelli for their contribution to the project as part of their student activities. Fruitful discussions with Tommaso Andreussi, Gianni Pellegrini, and Niccola Kutufà are also greatly acknowledged. We would also like to thank Giovanni Pace for supplying the Bronkhorst mass flow meter.

Conflicts of Interest: The authors declare no conflict of interest.

References

1. Szabo, J.; Robin, M.; Paintal, S.; Pote, B.; Hruby, V. High Density Hall Thruster Propellant Investigations. In Proceedings of the 48th AIAA/ASME/SAE/ASEE Joint Propulsion Conference—Exhibit, American Institute of Aeronautics and Astronautics, Atlanta, GA, USA, 30 July–1 August 2012. [[CrossRef](#)]
2. Betzendahl, R. *Rare Gases: A Fast Growing Global Commodity*; CryoGas International: Lexington, MA, USA, 2007.
3. Linnell, J.; Gallimore, A. Efficiency Analysis of a Hall Thruster Operating with Krypton and Xenon. In Proceedings of the 41st AIAA/ASME/SAE/ASEE Joint Propulsion Conference and Exhibit, American Institute of Aeronautics and Astronautics, Tucson, AZ, USA, 10–13 July 2005. [[CrossRef](#)]
4. Dankanich, J.; Szabo, J.J.; Pote, B.; Oleson, S.R.; Kamhawi, H. Mission and System Advantages of Iodine Hall Thrusters. In Proceedings of the 50th AIAA/ASME/SAE/ASEE Joint Propulsion Conference, American Institute of Aeronautics and Astronautics, Cleveland, OH, USA, 28–30 July 2014. [[CrossRef](#)]
5. Szabo, J.; Robin, M.; Paintal, S.; Pote, B.; Hruby, V.; Freeman, C. Iodine Plasma Propulsion Test Results at 1–10 kW. *IEEE Trans. Plasma Sci.* **2015**, *43*, 141–148. [[CrossRef](#)]

6. Tverdokhlebov, O.; Semenkin, A. Iodine propellant for electric propulsion—To be or not to be. In Proceedings of the 37th Joint Propulsion Conference and Exhibit, American Institute of Aeronautics and Astronautics, Salt Lake City, UT, USA, 8–11 July 2001. [[CrossRef](#)]
7. Branam, R. *Iodine Plasma (Electric Propulsion) Interaction with Spacecraft Materials—AFRL-AFOSR-VA-TR-2016-0381*; Technical report; Air Force Research Laboratory: Wright-Patterson Air Force Base, OH, USA, 2016.
8. Paganucci, F.; Saravia, M.M.; Mininni, M.; Bernazzani, L.; Ceccarini, A.; Boulzaguet, T.; Pellegrini, G.; Ducci, C.; Pedrini, D.; Andreussi, T.; et al. Progress on the Development of an Iodine-fed Hall Effect Thruster. In Proceedings of the 35th International Electric Propulsion Conference, Georgia Institute of Technology, Atlanta, GA, USA, 8–12 October 2017; IEPC-2017-418.
9. McLean, C.H.; Webb, S.D.; Onursal, C.A.; Ralea, M.; Stolan, J.A. Development of a Flight Propellant Regulation System for Hall Effect Thrusters. In Proceedings of the 27th International Electric Propulsion Conference, Pasadena, CA, USA, 14–19 October 2001; IEPC-01-321.
10. Bober, A.; Kozubsky, K.; Komarow, G.; Maslennikov, N.; Kozlov, A.; Romashko, A. Development and Qualification Test of a SPT Electric Propulsion System for “GALS” Spacecraft. In Proceedings of the 23rd International Electric Propulsion Conference, Seattle, WA, USA, 12–17 September 1993; IEPC-93-008.
11. Bushway, E.D., III; Engelbrecht, C.S.; Ganapathi, G.B. NSTAR Ion Engine Xenon Feed System: Introduction to System Design and Development. In Proceedings of the 25th International Electric Propulsion Conference, Cleveland, OH, USA, 24–28 August 1997; IEPC-97-044.
12. Aadland, R.S.; Engelbrecht, C.S.; Ganapathi, G.B.; Browning, D.A.; Wilson, F.; Hoskins, W.A. Xenon Propellant Management System for 40 cm NEXT Ion Thruster. In Proceedings of the 39th AIAA/ASME/SAE/ASEE Joint Propulsion Conference and Exhibit, Huntsville, AL, USA, 20–23 July 2003; AIAA-2003-4880.
13. Szabo, J.J., Jr.; Pote, B.; Paintal, S.; Robin, M.; Hruby, V. Iodine Fueled Plasma Generator System. U.S. Patent 8,610,356B2, 17 December 2013.
14. Dressler, R.A.; Levandier, D.J.; Chiu, Y.H. Iodine Electric Propulsion Thrusters. U.S. Patent 6,609,363B1, 26 August 2003.
15. Polzin, K.A.; Peeples, S.R.; Seixal, J.F.; Mauro, S.L.; Lewis, B.L.; Jerman, G.A.; Calvert, D.H.; Dankanich, J.; Kamhawi, H.; Hickman, T.A.; et al. Propulsion System Development for the Iodine Satellite (iSAT) Demonstration Mission. In Proceedings of the 34th International Electric Propulsion Conference, Kobe-Hyogo, Japan, 6–10 July 2015; IEPC-2015-09/ISTS-2015-b-09.
16. Tsay, M.; Frongillo, J.; Hohman, K. Iodine-Fueled Mini RF Ion Thruster for CubeSat Applications. In Proceedings of the Joint Conference of 30th International Symposium on Space Technology and Science 34th International Electric Propulsion Conference and 6th Nano-satellite Symposium, Hyogo-Kobe, Japan, 4–10 July 2015; IEPC-2015-273 /ISTS-2015-b-273.
17. *NIST Standard Reference Database Number 69*; NIST: Gaithersburg, MD, USA, May 2018.
18. Polzin, K.A.; Peeples, S.R.; Martinez, A.; Seixal, J.F.; Mauro, S.; Burt, A.O.; Myers, J.L. Engineering Model Propellant Feed System Development for an Iodine Hall Thruster Demonstration Mission. In Proceedings of the 52nd AIAA/SAE/ASEE Joint Propulsion Conference, American Institute of Aeronautics and Astronautics, Salt Lake City, UT, USA, 25–27 July 2016. [[CrossRef](#)]
19. Idel’chik, I.; Steinberg, M. *Handbook of Hydraulic Resistance*; CRC Press: Boca Raton, FL, USA, 1994.
20. Ascher, H.; Shapiro, R.E.S. *The Dynamics and Thermodynamics of Compressible Fluid Flow*; John Wiley & Sons, Inc.: Hoboken, NJ, USA, 1953.
21. White, F.M. *Viscous Fluid Flow*, 2nd ed.; McGraw-Hill, Inc.: New York, NY, USA, 1991.
22. Chung, T.H.; Lee, L.L.; Starling, K.E. Application of Kinetic Gas Theories and Multiparameter Correlation for Prediction of Dilute Gas Viscosity and Thermal Conductivity. *Ind. Eng. Chem. Res.* **1984**, *23*, 8–13. [[CrossRef](#)]
23. Chung, T.H.; Mohammad, A.; Lee, L.L.; Starling, K.E.; Ajlan, M. Generalized Multiparameter Correlation for Nonpolar and Polar Fluid Transport Properties. *Ind. Eng. Chem. Res.* **1988**, *27*, 671–679. [[CrossRef](#)]
24. Reid, R.C.; Prausnitz, J.M.; Poling, B.E. *The Properties of Gases & Liquids*; McGraw-Hill: New York, NY, USA, 1987.
25. Neufeld, P.D.; Janzen, A.R.; Aziz, R.A. Empirical equations to calculate 16 of the transport collision integrals $\Omega(l,s)^*$ for the Lennard-Jones (12-6) potential. *J. Chem. Phys.* **1972**, *57*, 1100–1102. [[CrossRef](#)]
26. Mason, E.A.; Monchick, L. Transport properties of polar-gas mixtures. *J. Chem. Phys.* **1962**, *36*, 2746–2757. [[CrossRef](#)]

27. Dose, V. Bayesian inference in physics: Case studies. *Rep. Prog. Phys.* **2003**, *66*, 1421–1461. [[CrossRef](#)]
28. Sivia, D.; Skilling, J. *Data Analysis: A Bayesian Tutorial*; Oxford Science Publications: Oxford, UK, 2006.
29. Veitch, J.; Vecchio, A. Bayesian coherent analysis of in-spiral gravitational wave signals with a detector network. *Phys. Rev. D* **2010**, *81*. [[CrossRef](#)]
30. Pitkin, M.; Romano, J. Available online: <https://ccpforge.cse.rl.ac.uk/gf/project/multinest> (accessed on 1 February 2017).
31. Bergman, T.L.; Lavine, A.S.; Incropera, F.P.; DeWitt, D.P. *Fundamentals of Heat and Mass Transfer*; Wiley: Hoboken, NJ, USA, 2011.
32. Paganucci, F.; Bernazzani, L.; Ceccarini, A.; Saravia, M. Development of an Iodine Feeding System for Low Power Ion and Hall Effect Thrusters. In Proceedings of the AIAA Propulsion and Energy 2019 Forum, American Institute of Aeronautics and Astronautics, Indianapolis, IN, USA, 19–22 August 2019. [[CrossRef](#)]
33. Paganucci, F.; Saravia, M.; Pedrini, D.; Bernazzani, L.; Ceccarini, A. Development of an Iodine Propellant Feeding System for Electric Propulsion. In Proceedings of the 5th Space Propulsion Conference, Rome, Italy, 2–6 May 2016.
34. Rankine, A.O. On the Viscosity of the Vapour of Iodine. *Proc. R. Soc. A Math. Phys. Eng. Sci.* **1915**, *91*, 201–208. [[CrossRef](#)]
35. Saravia, M.M. Alternative Propellants for Hall Thrusters. Ph.D. Thesis, Università di Pisa, Pisa, Italy, 2019.



© 2020 by the authors. Licensee MDPI, Basel, Switzerland. This article is an open access article distributed under the terms and conditions of the Creative Commons Attribution (CC BY) license (<http://creativecommons.org/licenses/by/4.0/>).